# A mechanistic understanding of the wear coefficient: From single to multiple asperities contact

Lucas Frérot[a,*], Ramin Aghababaei[a,b], Jean-François Molinari[a]

[a] *Institute of Civil Engineering, École Polytechnique Fédérale de Lausanne (EPFL), CH 1015 Lausanne, Switzerland*
[b] *Department of Engineering — Mechanical Engineering, Aarhus University, 8000 Aarhus, Denmark*

**Abstract**

Sliding contact between solids leads to material detaching from their surfaces in the form of debris particles, a process known as wear. According to the well-known Archard wear model, the wear volume (i.e. the volume of detached particles) is proportional to the load and the sliding distance, while being inversely proportional to the hardness. The influence of other parameters are empirically merged into a factor, referred to as wear coefficient, which does not stem from any theoretical development, thus limiting the predictive capacity of the model. Based on a recent understanding of a critical length-scale controlling wear particle formation, we present two novel derivations of the wear coefficient: one based on Archard's interpretation of the wear coefficient as the probability of wear particle detachment and one that follows naturally from the up-scaling of asperity-level physics into a generic multi-asperity wear model. As a result, the variation of wear rate and wear coefficient are discussed in terms of the properties of the interface, surface roughness parameters and applied load for various rough contact situations. Both new wear interpretations are evaluated analytically and numerically, and recover some key features of wear observed in experiments. This work shines new light on the understanding of wear, potentially opening a pathway for calculating the wear coefficient from first principles.

*Keywords:* wear coefficient; contact; cluster statistics; self-affine surface

## 1. Introduction

The scientific study of wear dates back to the early 19$^{\text{th}}$ century [18], but our current understanding was built upon research conducted in the middle of the last century [5]. Wear comes in various forms, with adhesive wear, the process of detachment of surface asperities tip by adhesive forces during the sliding contact of two solids, being one of the most prominent. Systematic wear experiments in the mid-20$^{\text{th}}$ century [3, 6] suggested a general relation where the wear rate (i.e. wear volume per unit sliding distance) is linearly proportional to the applied normal load, in a certain range of the latter [6, 43], and related to the hardness of the material. Inspired by this experimental evidence, Archard [3] generalized Holm's concept of "atom removal" [20] to "debris removal" and pictured an adhesive wear model. He assumed that an asperity junction of radius $a$ produces a debris volume proportional to $a^3$ over an effective sliding distance of $2a$, giving a linear relationship between wear rate and real contact area at the asperity level. To extend this single-asperity relation to a multi-asperity contact, Archard argued that only a fraction of contacting asperities, a quantity referred to as the "wear coefficient", produces wear particles. This conception of the "wear coefficient" being key in understanding wear, Archard and Hirst [4] claimed that "...one of the most important problems in an understanding of wear is to explain the magnitude of the probability of the production of a wear particle at an asperity encounter." This long-standing problem has remained

*Corresponding Author
*Email addresses:* lucas.frerot@epfl.ch (Lucas Frérot), aghababaei@eng.au.dk (Ramin Aghababaei), jean-francois.molinari@epfl.ch (Jean-François Molinari)

unresolved, and evaluation of the wear coefficient is still relying on empirical data, with no insight from a physical model.

Similarly to the friction coefficient [47], the wear coefficient is a system property that depends on many parameters including applied load [51, 44], material properties of sliding bodies (e.g. fracture toughness [15, 9]) and properties of interface (e.g. dry or lubricated contact [25], roughness parameters [25], chemical properties [32]). However, all these effects are currently empirically merged into the wear coefficient, which limits the applicability of Archard's model. Therefore, our goal in this work is to further the understanding of adhesive wear in multi-asperity setting, based on a physics-based understanding of the wear process. To this effect, we base our approach on the concept of critical length-scale governing the formation of wear particles [1]. This concept stems from energy balance between the available deformation energy in an asperity encounter and the energy required to detach a wear particle [17, 41, 42]. The balance states that contacts smaller than a critical length-scale $d^*$ plastically deform and contacts larger than $d^*$ break into a wear particle. This was recently shown with molecular dynamics simulations [1]. The critical length-scale $d^* = \lambda \cdot G\Delta w/\sigma_j^2$ is function of the shear modulus $G$, the fracture energy per unit area $\Delta w$ and the junction strength $\sigma_j$ with a shape factor $\lambda$, all of which can be determined by direct experiments or analytical predictions, with no fit parameter.

In this article, we present two new conceptions of the wear coefficient that is built upon the critical length-scale concept. The first concept incorporates Archard's interpretation of the wear coefficient as the "probability of production of a wear particle". The second is based on an up-scaling of single-asperity wear considerations to a multi-asperity contact setting. Both concepts are analytically and numerically studied in different contact situations. We compare them in the context of contact of self-affine surfaces and show that the concept based on Archard's interpretation leads to a constant coefficient wear within a certain range of load, while the second does not. We finally give possible explanations as to why this is the case, and potential improvements to the proposed models.

## 2. Review of Archard's wear model

Archard's wear model [3] can be decomposed into two parts: the single-asperity wear model and the contact model. At the single asperity level, the amount of material removed in an asperity interaction is considered proportional to $a^3$ ($a$ is the asperity contact radius), whereas the sliding distance required to break off the wear particle is proportional to $a$. This gives the general relationship for the wear rate (worn volume per sliding distance) of a single asperity (subscript 1, see Table 1):

$$R_1 = \omega A \tag{1}$$

where $A$ is the contact area of the asperity and $\omega$ is a generic shape factor, equal to $1/3$ in the case of spherical asperities forming hemi-spherical wear particles. This hypothesis is discussed in [42] and has been verified for isolated debris with molecular dynamics [2]. At the multi-asperity level, Archard makes two hypotheses:

I. the size and shape of the individual contact areas are given by a contact model considering a rough surface made of spheres with radius $r$ uniformly distributed in depth, with density $d$ (number of spheres per unit distance).

II. a probability factor $K$ applies on each contact to account for the fact that not all asperity encounters result in a wear particle. Archard assumes $K$ is independent of $a$.

Using these, the global wear can be related to the applied load $W$:

$$\begin{aligned} R(W) &= K\omega A_c(W) \\ &= K\frac{\omega b d}{2}\left(\frac{p+1}{cd}W\right)^{\frac{2}{p+1}} \end{aligned} \tag{2}$$

Table 1: Symbols and notations

| Symbol | Description | Physical dimension |
|---|---|---|
| $A$ | single asperity contact area | area |
| $R$ | wear rate | volume/distance |
| $W, \delta$ | normal applied load, indentation depth | force, distance |
| $d^*, A^*$ | critical length-scale, critical area | distance, area |
| $(\cdot)_1$ | quantity relative to a single asperity contact | — |
| $K$ | wear coefficient based on Archard's interpretation | dimensionless |
| $\mathcal{K}$ | wear coefficient based on up-scaling approach | dimensionless |
| $(\cdot)_{\mathrm{PL}}$ | quantity computed with power-law contact model | — |
| $(\cdot)_{\mathrm{num}}$ | quantity numerically computed | — |
| $A_c$, $A_c^*$ | real contact area, cumulated area of contacts larger than $A^*$ | area |
| $p(X, y)$ | probability density function of random variable $X$ with parameter $y$ | dimension of $1/X$ |
| $P(X > x, y)$ | probability of the event $X > x$ with parameter $y$ | dimensionless |
| $N$ | number of contacts | dimensionless |
| $\lambda_l$, $\lambda_s$ | largest and smallest wavelengths | distance |
| $H$ | Hurst exponent | dimensionless |
| $L$, $\Delta l$ | system size, discretization | distance |
| $d$ | height density | 1/distance |
| $A_s$, $A_m$ | smallest and largest micro-contact areas | area |
| $\alpha$, $C$ | power-law exponent and plateau value | dimensionless, 1/area |
| $E$, $\nu$, $\mathcal{H}$ | Young's modulus, Poisson's ratio, indentation hardness | pressure, dimensionless, pressure |
| $E^\star$ | effective Young's modulus ($E^\star \equiv E/(1-\nu^2)$) | pressure |
| $G$, $\Delta w$, $\sigma_j$ | shear modulus, adhesive energy per unit area, junction shear strength | pressure, energy/area, pressure |

where $A_c$ is the true contact area, $b$, $c$ and $p$ are found in table 2. In the case of a rigid-plastic material the wear equation is a linear relationship written as:

$$R(W) = K\omega \cdot \frac{W}{\mathcal{H}} \tag{3}$$

| Behavior | $b$ | $c$ | $p$ |
|---|---|---|---|
| Elastic | $\pi r$ | $4.25E\sqrt{r}$ | $\frac{3}{2}$ |
| Plastic | $2\pi r$ | $2\pi r\mathcal{H}$ | 1 |

Table 2: Parameters for Archard's multi-asperity contact model. $E$ is the Young's modulus, $\mathcal{H}$ is the hardness of the material and $r$ is the radius of the spherical asperities.

Equation (2) shows that the total wear rate is proportional to the total contact area, with a proportionality factor $K$ (modulo a shape factor), and equation 3 recovers the experimentally-observed linear relationship between wear rate and load [6] (within a certain load interval). The wear equation is however non-linear in any other case than rigid-plastic behavior. This limitation comes exclusively from Archard's contact model, as it governs the $W \mapsto A_c$ relationship. Note that other contact models [16, 36] would yield a linear $W \mapsto A_c$ relationship in the purely elastic case.

## 3. Wear coefficients based on critical length-scale

Archard interprets the proportionality factor as the probability that a given asperity encounter yields a wear particle, and introduces it at the asperity level by expressing the single asperity wear rate as $R_1 = K\omega A$. This suggests that the particle formation is a random process at the asperity level and independent of the micro-contact size. This is inconsistent with recent results [1] that exhibit a Griffith-like criterion governing the detachment of wear particles for homogeneous materials, the latter thus being deterministic.

We now fundamentally enrich Archard's interpretation of the wear coefficient by considering, within a multi-contact setting, a critical micro-contact area:

$$A^* \propto \left(\frac{G\Delta w}{\sigma_j^2}\right)^2 \tag{4}$$

which is the square of the critical length-scale defined in [1]. This length-scale is derived from the balance of available deformation energy and required energy to form a wear particle. In this expression, $G$ is the shear modulus, $\Delta w$ is the fracture energy per unit area and $\sigma_j$ is the asperity junction's shear strength. We now complement the equation (2) with two new statements:

A. the size and shape of individual contacts are the outcome of contact between random surfaces. The area of a single contact (also called contact cluster) is a random variable $A$ characterized by a probability density function $p(A, W)$.

B. The process of debris formation is deterministic at the asperity level. It is governed by a critical area $A^*$: if the area $A$ of a cluster is larger than $A^*$, a wear particle is formed (figure 1).

With this, we are now in position to propose two alternative definitions of the wear coefficient.

### 3.1. Wear coefficient based on Archard's interpretation

Archard's interpretation of the wear coefficient is the "probability of the production of a wear particle at an asperity encounter". With the critical area $A^*$ in mind, the probability of production of a wear particle is simply:

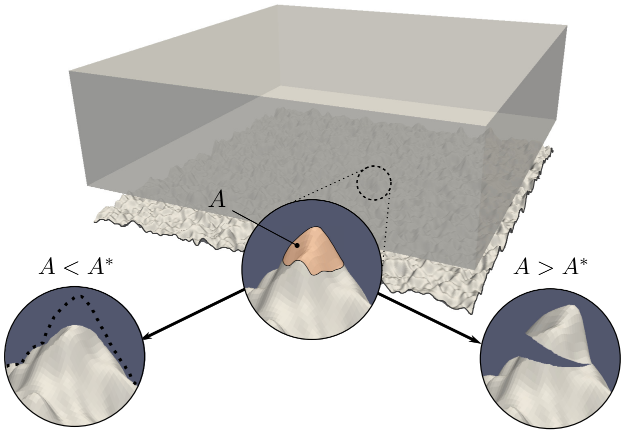


Figure 1: **Schematic representation of rough contact and corresponding wear mechanisms.** A contact cluster forms a wear particle upon sliding if its area is larger than $A^*$, otherwise the asperity in contact deforms upon sliding without breaking (hypothesis B). This hypothesis brings asperity-level physics in the wear particle formation process through the critical cluster size $A^*$.

$$K \equiv P(A > A^*, W) = \int_{A^*}^{\infty} p(A, W)\,\mathrm{d}A \tag{5}$$

which is the probability that a realization of the random variable $A$ is larger than $A^*$ for a given load $W$. This definition maintains Archard's interpretation of the wear coefficient while defining it at the multi-asperity level.

### *3.2. Alternative formulation of wear coefficient*

Although Archard's interpretation of the wear coefficient is widely accepted, and therefore of prime interest, it is not physically justified by Archard, and still relies on a direct sum of wear volume produced by every micro-contact (weighted by a constant probability coefficient), which is not compatible with the critical length-scale concept. Here, we propose a new interpretation of the wear coefficient: we directly use the single asperity wear relation of equation (1) with no probability coefficient and sum the wear rate of all contacts forming a wear particle, thus truly up-scaling equation (1) to multi-asperity contact.

Considering a system of finite size, there is a finite number $N(W)$ of clusters in the system. We define $n(A, W) \equiv N(W) \cdot p(A, W)$. Provided $A \mapsto An(A, W)$ is integrable on $[0, +\infty[$, we can compute the total wear rate, using Archard's single-asperity wear rate and the critical length-scale concept, as a weighted sum of all contacts larger than $A^*$:

$$R(W) = \int_{A^*}^{\infty} R_1(A) n(A, W)\,\mathrm{d}A = \int_{A^*}^{\infty} \omega A n(A, W)\,\mathrm{d}A = \omega A_c^*(W) \tag{6}$$

where $A_c^*$ is the cumulated area of all clusters forming a wear particle and $\omega$ is an average shape factor. We define the function $\mathcal{K}(W)$ as:

$$\mathcal{K}(W) \equiv \frac{A_c^*(W)}{A_c(W)} = \frac{\int_{A^*}^{\infty} Ap(A, W)\,\mathrm{d}A}{\int_{0}^{\infty} Ap(A, W)\,\mathrm{d}A} \tag{7}$$

where $A_c(W)$ is the total contact area. This allows us to write the wear rate as $R(W) = \mathcal{K}(W)\omega A_c(W)$, in the same form as equation (2). We call $\mathcal{K}(W)$ the "wear coefficient", but its definition is substantially different from Archard's, as we now have an area ratio instead of a probability of particle formation. The definition in equation (7) results naturally from the up-scaling of the single-asperity wear considerations to multi-asperity contact, unlike Archard's wear coefficient, which was introduced *a posteriori* into the wear rate equation.

## 4. Numerical results

Without making *a priori* assumptions on the distribution of cluster areas, numerical simulation allows the direct application of the wear models on realistic surfaces [37]. We evaluate the wear coefficient and the wear rate using a model for rough-surface contact consisting of a flat, semi-infinite elastic medium in contact with a rigid solid having a random rough surface. The contact problem is solved using a boundary-element approach [46, 38] which fully accounts for elastic interactions. The wear coefficient is investigated through the analysis of the contact map across a representative sample of simulations. The area of each contact cluster is determined from the contact map using an 8-neighbors flood-fill algorithm[1]. This approach allows a direct computation of the wear coefficient using equation (5) and (7).

The rough surfaces are random self-affine (fractal) isotropic surfaces [31, 34], with height function $h(x, y)$ generated by a filtering algorithm [22]. They are defined through their power spectral density (PSD). The surfaces are isotropic, so the surface PSD depends only on the radial coordinate $q = 2\pi/\lambda$, where $\lambda$ is a wavelength. The surface PSD is defined using $\lambda_s$, $\lambda_l$, respectively the short wavelength cut-off and the large wavelength cut-off [34, 49]. Between $q_l = 2\pi/\lambda_l$ and $q_s = 2\pi/\lambda_s$, the PSD decays as $q^{-2(H+1)}$. $H$ is the Hurst exponent, governing the self-affine behavior of the fractal rough surface. We vary the Hurst exponent between 0.6 and 0.8 as is commonly occurring in natural surfaces [37]. There are three main properties governing the statistics of fractal surfaces:

- $L/\lambda_l$ where $L$ is the size of the surface, governs the representativity of the surface [49]. A large value yields a surface with many large asperities, allowing better statistics while also reducing the effect of the periodic boundary conditions.
- $\lambda_l/\lambda_s$ controls the range of the PSD. This quantity influences the spectrum bandwidth of the surface [34].
- $\lambda_s/\Delta l$, where $\Delta l$ is the discretization size, governs the discretization error which causes bias in evaluated mechanical and statistical quantities, but also governs the resolution of the details of the fractal contact clusters [50]. A large value reduces both of these sources of error.

Figures B.1 and B.2 show a sensitivity analysis that justifies the use of $L/\lambda_l = \lambda_s/\Delta l = 8$ in the work presented. All data obtained from simulation is normalized by $\lambda_s$ for lengths and $W_0 = E^\star\sqrt{\langle|\nabla h|^2\rangle}L^2$ for loads, where $E^\star$ is the effective Young's modulus and $\sqrt{\langle|\nabla h|^2\rangle}$ is the standard deviation of surface slopes. Figure 2a shows one realization of this surface. Figures 2b-d show the contact map for different load steps in the range $W/W_0 \in [0.001, 0.2]$, indicated by dashed lines in figure 2e. Black area is not in contact, yellow contact clusters are smaller than $A^*$, and red clusters are larger. As the load is increased, clusters grow to span more of the available area, occasionally merging to form larger clusters, as shown in figure 2e with the increase in contact area and maximum cluster size. The latter increases dramatically as the clusters merge, forecasting percolation. Figure 2f represents the increase in the number of clusters per increase of contact area ($\mathrm{d}N/\mathrm{d}A_c$). Positive values indicate the regime where contact-area growth is dominated by nucleation of clusters, and negative values indicate the regime where cluster merging dominates contact-area growth. We focus our study to the former regime, in which the clusters are far enough to neglect interactions in the debris forming process. As postulated by Burwell and Strang [6], this corresponds to the mild wear regime [48, 12, 19]. We let $W/W_0 \in [0.001, 0.06]$, discretized in thirty load steps for the other simulations presented in this paper.

### *4.1. Statistical distribution of contact clusters*

Figure 3 presents the probability density function of cluster areas at multiple applied loads for three different spectrum range parameters ($\lambda_l/\lambda_s$) and a Hurst exponent of 0.8. Results for different Hurst exponents and $\lambda_l/\lambda_s = 128$ are shown in the inset. In agreement with previous experimental observations [29,

[1] neighborhood definition has no influence on distribution of cluster areas when discretization is fine enough.

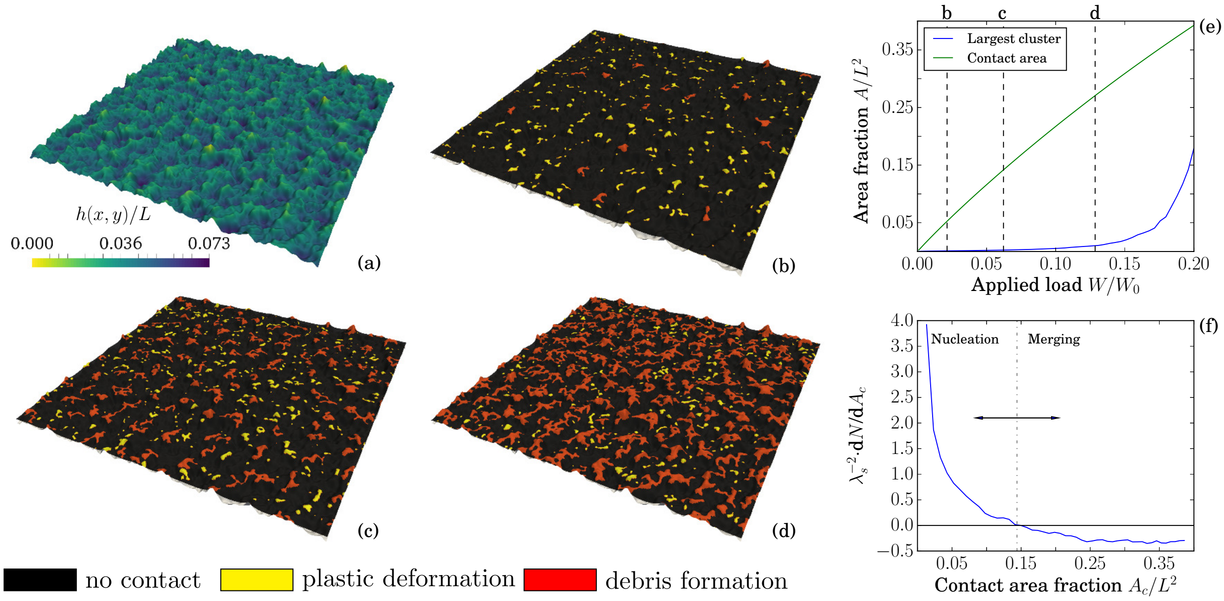


Figure 2: **Evolution of contact area with increasing normal load.** Simulation of forty realizations with $\lambda_l/\lambda_s = 8$ and fifty load steps in $[0.001, 0.20] \cdot W_0$. $A^*$ is taken as $2\lambda_s^2$. (a) shows a rough surface sample. (b), (c) and (d) show the state of one realization at the loads indicated by dashed lines in (e). The video provided with the supplementary material shows the contact evolution for this realization. It can be seen from (b), (c) and (d) that the number and the size of clusters increase with $W$. (e) shows the combined effect of those two contact-area growth mechanisms on the total contact area $A_c$. It also shows the size of the largest cluster, which increases dramatically when the growth of $A_c$ is dominated by cluster merging. Figure (f) shows the rate of increase in the number of clusters with respect to $A_c$. Positive values indicate a regime where the growth of $A_c$ is dominated by cluster nucleation and negative values indicate that the merging of clusters dominates the contact-area growth.

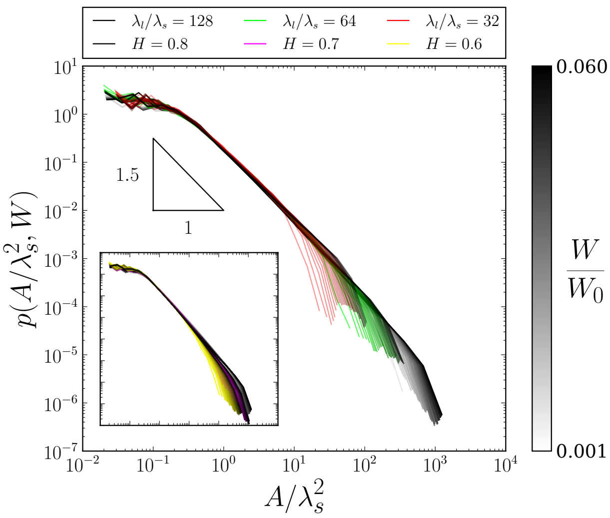


Figure 3: **Distribution of contact cluster areas.** The main graph shows $p(A/\lambda_s^2, W)$, the probability density function of normalized cluster areas for $H = 0.8$ and varying $\lambda_l/\lambda_s$, evaluated using twenty logarithmic bins. The inset shows the probability density function for values of $H \in \{0.6, 0.7, 0.8\}$ with $\lambda_l/\lambda_s = 128$. $p(A, W)$ can be approximated by a power-law within a certain cluster size interval, inside which it is independent of the applied load $W$. Increasing $W$ or $\lambda_l/\lambda_s$ increases the upper bound of the power-law interval. Normalization with the smallest wavelength $\lambda_s$ collapses all distributions to a single curve within the power-law interval. Varying the Hurst exponent has a limited effect on the resulting distribution.

14] and numerical simulations [23, 35, 8], the probability density function of cluster areas follows a power-law in a given interval of $A$. The evaluated exponent value of 1.5 (using a maximum likelihood estimator [10]) is well within the measured range of $1.05-2.69$ from the experiments of Dieterich and Kilgore [14], close to values of 1.6 predicted by the overlap model [30] and $1.54-1.56$ measured in the experiments of Majumdar and Bhushan [28]. Values predicted by various contact mechanics models (discrete and continuous) fully accounting for long-range asperity interactions are in the range of $1.45-1.6$ [24, 7, 33].

Figure 3 also shows that the behavior of $p(A, W)$ is independent of $W$ within the power-law interval, and that the upper bound of this interval increases with the load, in agreement with experimental observations [29]. The upper bound of the power-law interval is also increasing with the surface PSD range. Moreover, when cluster sizes are normalized with the shortest wavelength in the system, all probability density functions collapse to a single curve within the power-law interval. The inset of figure 3 shows that the Hurst exponent has limited influence on the distribution of clusters and only affects the fall-off behavior at large cluster areas, making the power-law approximation less accurate in this range.

### *4.2. Wear coefficient*

Figure 4a shows the wear coefficient, $K_{\mathrm{num}}$, as defined in equation (5). It exhibits common features with figure 3, namely a power-law behavior in a given interval of $A^*$ and the increase of the upper bound of that interval with $W$ and with $\lambda_l/\lambda_s$. The load-invariant power law of figure 4a signals a constant wear coefficient for a given load range. Figure 4b shows the evolution of the wear coefficient as a function of load (surface used has $\lambda_l/\lambda_s = 128$). Remarkably, regardless of $A^*$, the wear coefficient transitions from zero (i.e. no observable wear) to a constant value given by the power law of figure 4a, which corresponds to the proportionality constant observed in experiments [5, 43, 4]. This is the first time to our knowledge that a model derived from first principles predicts a constant wear coefficient within a given load range and a transition from no observable wear (i.e. wear coefficient is zero) to mild wear (i.e. wear coefficient is constant). This transition occurs at a critical load that depends on the value of $A^*$, and is larger for systems with higher $A^*$ (as would be the case in lubricated contact). For systems with small $A^*$ values (e.g. poor lubrication conditions), the critical load may be lower than the lowest load we simulate. Note that in the presence of lubrication, the wear volume is affected by a change of $A^*$ as well as a reduction of the solid contact area.

Figure 5a and 5b show the wear coefficient $\mathcal{K}_{\mathrm{num}}$ and the wear rate as functions of the load, computed from equations (6) and (7) respectively. Figure 5a shows that the wear coefficient is zero up to a transition load that depends on $A^*$. For $A^*$ in the low range of values we simulate, the transition load is smaller than $0.001 \cdot W_0$. Similarly to Archard's wear coefficient, this new interpretation is able to exhibit the no-wear/wear transition that has been observed in experiments [11]. After the transition load, the wear coefficient increases monotonically up to one. In figure 5b, the wear rate is quasi-linear after a transition region [26].

Although there is a qualitative agreement of equation (5) with experimental observation, a quantitative agreement is difficult to obtain because measurements of hardness and RMS of slopes are difficult and not systematic in wear experiments. In the experiments of Burwell and Strang [6], good care is taken in eliminating all possible sources of wear but adhesive wear, and they provide a good base for a quantitative comparison. However no precise estimation of the wear coefficient is given. They nonetheless give measurements of the transition load to severe wear, which is the limit of our model, and thus cannot be computed using our base assumptions that neglect asperity interactions during the wear process.

### *4.3. Analytical results*

In order to understand the properties of the proposed wear coefficients in the contact of self-affine surfaces, we develop analytical expressions of $K$ and $\mathcal{K}$ for a power-law distribution of contact clusters, as suggested by figure 3:

$$p_{\mathrm{PL}}(A, A_m) = \begin{cases} C & A \in [0, A_s] \\ C\left(\dfrac{A}{A_s}\right)^{-\alpha} & A \in [A_s, A_m] \\ 0 & A \in [A_m, +\infty) \end{cases} \tag{8}$$

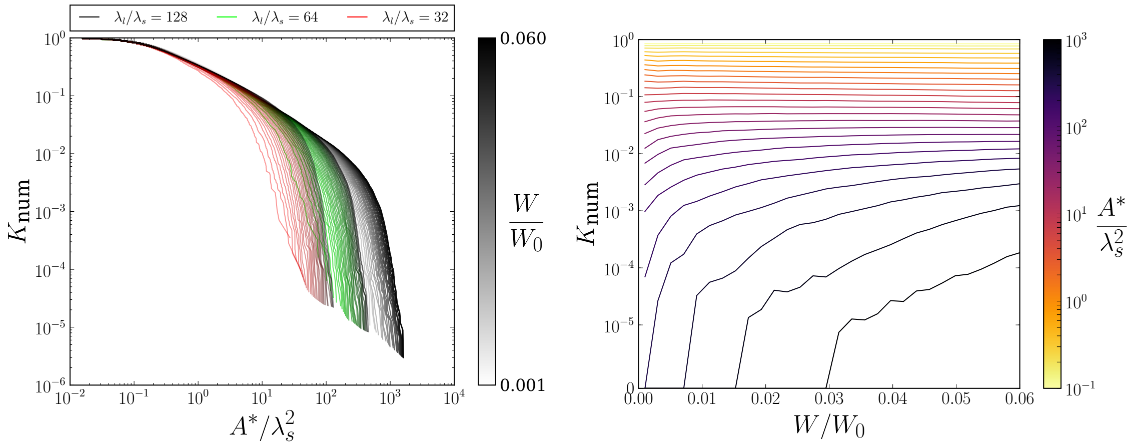


(a)

(b)

Figure 4: **Archard's wear coefficient in context of self-affine surface contact.** (a) shows the complementary cumulative probability distribution function ($H = 0.8$), (b) shows Archard's wear coefficient as a function of the applied load (for $\lambda_l/\lambda_s = 128$ and $H = 0.8$). Regardless of $A^*$ there exists a critical load at which the wear coefficient transitions from zero (i.e. no wear debris) to a constant value (i.e. steady-state mild wear regime). This critical load largely depends on the value of $A^*$: the transition occurs at a higher critical load for contacts with lower interfacial shear strength and consequently larger $A^*$ (i.e. better lubrication condition). In (b) the y-axis is linear up to $10^{-5}$.

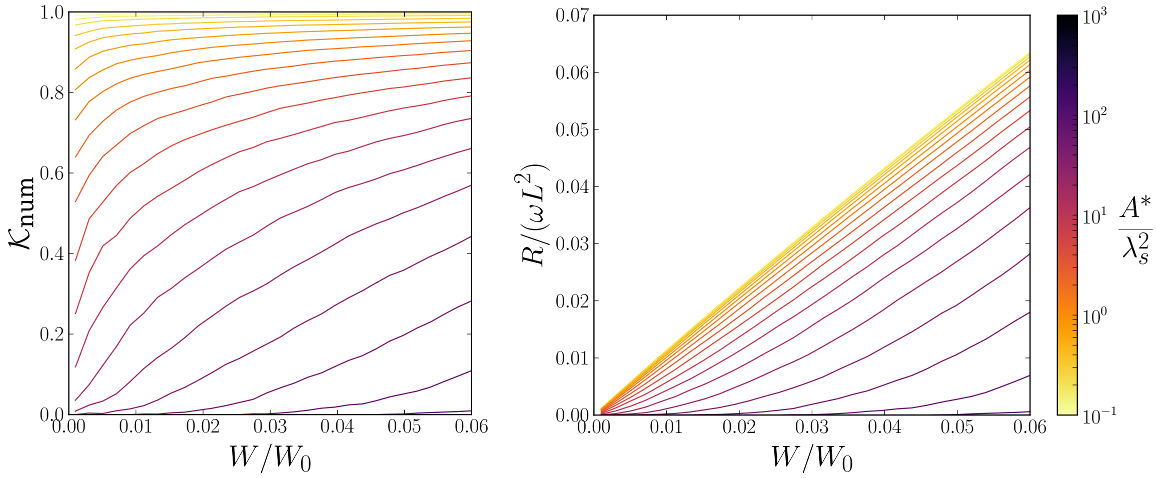


(a)

(b)

Figure 5: **Wear coefficient and wear rate** ($H = 0.8$ and $\lambda_l/\lambda_s = 128$). While the wear coefficient is non-constant with the load, its derivative decreases with the load. However, regardless of $A^*$, the limit value of $K$ is one, which does not correspond to experimental observations. Similarly, the wear rate is increasing non-linearly with the load, although its derivative stabilizes to a fixed value with increasing load.

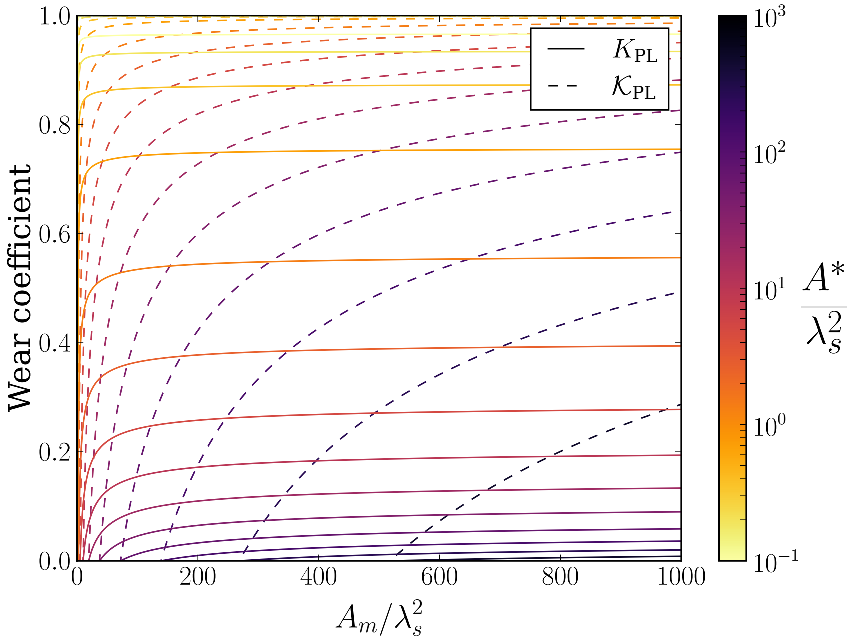


Figure 6: **Comparison between Archard's wear coefficient $K_{\mathrm{PL}}$ and the proposed interpretation $\mathcal{K}_{\mathrm{PL}}$ for a power-law distribution of cluster areas ($\alpha = 1.5$).** As can be seen in the expressions of equations (9) and (10), the behavior of $\mathcal{K}$ is different from $K$ when $\alpha < 2$: we have $\mathcal{K} \to 1$ whereas $K$ plateaus at values in $]0, 1[$.

$C$ is a normalizing factor such that $\int_0^\infty p_{\mathrm{PL}}(A, A_m)\,\mathrm{d}A = 1$ and $\alpha$ is the power-law exponent, set to the value measured in figure 3. The effect of increasing the contact load is taken into account via increasing $A_m$. Applying the previously stated equations for the wear coefficient yields the following expressions (c.f. Appendix A for details):

$$K_{\mathrm{PL}} = \begin{cases} 1 - \dfrac{A_s^{-\alpha}(1-\alpha)A^*}{A_m^{1-\alpha} - \alpha A_s^{1-\alpha}} & A^* \in [0, A_s] \\ 1 - \dfrac{(A^*)^{1-\alpha} - \alpha A_s^{1-\alpha}}{A_m^{1-\alpha} - \alpha A_s^{1-\alpha}} & A^* \in [A_s, A_m] \\ 0 & A^* \in [A_m, +\infty) \end{cases} \tag{9}$$

$$\mathcal{K}_{\mathrm{PL}} = \begin{cases} 1 - \dfrac{A_s^{-\alpha}(1-\frac{\alpha}{2})(A^*)^2}{A_m^{2-\alpha} - \frac{\alpha}{2} A_s^{2-\alpha}} & A^* \in [0, A_s] \\ 1 - \dfrac{(A^*)^{2-\alpha} - \frac{\alpha}{2} A_s^{2-\alpha}}{A_m^{2-\alpha} - \frac{\alpha}{2} A_s^{2-\alpha}} & A^* \in [A_s, A_m] \\ 0 & A^* \in [A_m, +\infty) \end{cases} \tag{10}$$

The graphs of these expressions are displayed in figure 6. It is apparent that the behavior of $K_{\mathrm{PL}}$ and $\mathcal{K}_{\mathrm{PL}}$ when $A_m$ increases is very different: while $K_{\mathrm{PL}}$ tends to a limit whose value depends on $A^*$, the limit value of $\mathcal{K}_{\mathrm{PL}}$ is one, regardless of $A^*$. This discrepancy is caused by the value of $\alpha \leq 2$. If $\alpha > 2$, then $\mathcal{K}_{\mathrm{PL}}$ has a finite limit dependent on $A^*$, exhibiting a wear coefficient independent of the load.

## 5. Discussion

The values predicted for Archard's wear coefficient (figure 4) are in the order of $10^{-5} - 10^{-1}$, which is in the range of values reported in experiments ($10^{-8} - 10^{-1}$ [42, 21]), especially values for dry sliding [4].

We have shown that the upper bound of the power-law interval in the wear coefficient increases with the range of the surface PSD ($\lambda_l/\lambda_s$). Due to computational limits, the maximum value of $\lambda_l/\lambda_s$ simulated was 128, much lower than values of $10^3$ and above measured on real surfaces [40, 27, 37]. We postulate that the range of predicted values for the wear coefficient could reach the lower experimental values for larger PSD ranges: if $\lambda_s$ is decreased, both the power-law interval upper bound and $A^*/\lambda_s^2$ are increased. Moreover, it has been shown [35] that an elasto-plastic constitutive behavior also increases the upper bound of the power-law interval, and an elasto-plastic behavior is expected to occur even at small loads [16, 29].

The newly proposed model for the wear coefficient (figure 5) introduces an interpretation that does not rely on Archard's assumption that the probability of wear particle formation is the same for all contacts, but does not predict the behavior commonly observed in experiments, as the wear coefficient tends to a value of one regardless of the critical length-scale. The value of the power-law exponent $\alpha = 1.5$ is the cause of this discrepancy: the integrals in (7) are dominated by the value of $A_m$, the largest cluster size. This can be seen in the expression for the self-affine model in equation (10). There is no definite reasoning on the origins of $\alpha$, as it depends on the spectrum of the surface, but also on constitutive behavior. A value of $\alpha > 2$ would make the limit value of $\mathcal{K}$ dependent on the critical length-scale and strictly smaller than one. It may be the case that under elasto-plastic constitutive assumption this would be satisfied [35], but it requires efficient numerical methods to be checked accurately. In addition, our contact model does not include transport of wear particles or relative movement of surfaces and possible reattachment. These aspects likely also change $p(A, W)$ and therefore change the properties of the wear coefficient.

The formation of a tribological layer [39, 45] may also change the debris formation process and geometrical as well as physical properties of the surfaces. This may induce lubrication and/or formation of a third body, which could be accounted for *via* the proper modifications of the contact model and the energies involved in the Griffith criterion for particle formation.

Conclusive experimental data for validation of our proposed models is difficult to obtain, as wear experiments often include several coupled physical phenomenon (e.g. adhesion, chemistry, temperature). The experiments of Burwell and Strang [6] manage to focus on adhesive wear only, and show that the wear coefficient should remain constant for a specific load range before increasing sharply with the load. They relate the transition load to the hardness, arguing that when the average applied pressure reaches $\mathcal{H}/3$, individual contacts and detached wear particles start interacting to form larger debris. We have shown that our simulations remain in the regime where the contact area growth is dominated by cluster nucleation. Individual contacts are not close enough for interaction, and the wear coefficient computed could be compared with a measurement done with an average pressure less than $\mathcal{H}/3$. However, the experiments of Burwell and Strang [6] lack precise measurements of the wear coefficient and surfaces' spectra, which make quantitative comparison impossible. Some wear experiments [40, 13] provide surface spectra, but do not observe the variations of the wear coefficient with the applied load, although the values reported by Power et al. [40] are close to 0.02 in a linear wear regime, which is in the range of values we observe.

Ideally, a validating wear experiment would provide spectrum measurement of the surface, study only adhesive wear of homogeneous materials (similarly to [6]) and give wear coefficient measurements with respect to the load. We hope that the ideas we put forth in our paper can encourage the experimental community to move towards this kind of experiments. In the meantime, we are optimistic that an elasto-plastic contact model may bring us closer to an experimental validation of those ideas.

Nonetheless, the new approach we describe both incorporates physical properties of the interface (e.g. surface energy, junction strength), geometrical and statistical properties of the surfaces in contact, while remaining generic with respect to the contact model. This leaves the possibility to tune the latter to advances in contact mechanics (e.g. elasto-plastic contact), but also real measurement of rough surfaces.

## 6. Conclusion

We have presented two physics-based interpretations for the adhesive wear coefficient. The use of the critical length-scale is the key ingredient in our approach, and the results obtained show common characteristics with experimental observations. In particular, the results based on Archard's assumption that the wear coefficient is the probability of wear particle formation exhibit a transition in the wear coefficient, after which it remains constant with load. We also propose a second interpretation based on a direct up-scaling of single asperity adhesive wear, and observe that the wear coefficient depends on load. We hypothesize that this is due to limitations in the contact model rather than the approach taken to derive the wear coefficient. We provide analytical results for both wear concepts in different simple contact situations that give a broad understanding of how the wear coefficient evolves with interface physical parameters and surface roughness.

## 7. Acknowledgments

All authors wish to acknowledge Dr. Guillaume Anciaux for the initial version of the contact code used in this work and development discussions, the financial support from the Swiss National Science Foundation (grant #162569, "Contact mechanics of rough surfaces"), and support from EPFL through the use of the facilities of its Scientific IT and Application Support Center.

## Appendix A. Analytical results

### *A.1. Power-law distribution of cluster areas*

Recent contact simulations [23, 35, 24, 7] and experiments [28, 14] have shown that, in contact with self-affine surfaces, the probability density of cluster areas is constant up to an area $A_s$, then follows a power-law of exponent $-\alpha$ in the interval $[A_s, A_m]$, where $A_m$ is the size of the largest cluster in the system and is the only parameter depending on the load (cf. figure 3 for additional numerical evidence). Consider the following probability density function for cluster areas:

$$p_{\mathrm{PL}}(A, A_m) = \begin{cases} C & A \in [0, A_s] \\ C\left(\dfrac{A}{A_s}\right)^{-\alpha} & A \in [A_s, A_m] \\ 0 & A \in [A_m, +\infty) \end{cases} \tag{A.1}$$

where $C$ is chosen to satisfy $\int_0^\infty p(A, W)\,\mathrm{d}A = 1$:

$$C = \frac{1-\alpha}{{A_s}^\alpha A_m^{1-\alpha} - \alpha A_s} \tag{A.2}$$

### *A.2. Wear coefficients based on Archard's interpretation*

$$\begin{aligned} K_{\mathrm{PL}} = \int_{A^*}^\infty p_{\mathrm{PL}}(A, A_m)\,\mathrm{d}A &= \begin{cases} C\left[\displaystyle\int_{A^*}^{A_s} \mathrm{d}A + \int_{A_s}^{A_m} \left(\frac{A}{A_s}\right)^{-\alpha} \mathrm{d}A\right] & A^* \in [0, A_s] \\ C\displaystyle\int_{A^*}^{A_m} \left(\frac{A}{A_s}\right)^{-\alpha} \mathrm{d}A & A^* \in [A_s, A_m] \\ 0 & A^* \in [A_m, \infty] \end{cases} \\ &= \begin{cases} 1 - \dfrac{A_s^{-\alpha}(1-\alpha)A^*}{A_m^{1-\alpha} - \alpha A_s^{1-\alpha}} & A^* \in [0, A_s] \\ 1 - \dfrac{(A^*)^{1-\alpha} - \alpha A_s^{1-\alpha}}{A_m^{1-\alpha} - \alpha A_s^{1-\alpha}} & A^* \in [A_s, A_m] \\ 0 & A^* \in [A_m, +\infty) \end{cases} \end{aligned} \tag{A.3}$$

*A.3. Wear coefficients based on up-scaling approach*

Let $D$ be:

$$D \equiv \int_0^{\infty} A p_{\mathrm{PL}}(A, A_m)\,\mathrm{d}A = C\left[\int_0^{A_s} A\,\mathrm{d}A + \int_{A_s}^{A_m} A\left(\frac{A}{A_s}\right)^{-\alpha}\mathrm{d}A\right]$$
$$= C\left(A_s + \frac{A_s^{\alpha}}{2-\alpha}(A_m^{2-\alpha} - A_s^{2-\alpha})\right) \tag{A.4}$$

$$\mathcal{K}_{\mathrm{PL}} = \frac{1}{D}\int_{A^*}^{\infty} A p_{\mathrm{PL}}(A, A_m)\,\mathrm{d}A = \begin{cases} \dfrac{C}{D}\left[\displaystyle\int_{A^*}^{A_s} A\,\mathrm{d}A + \int_{A_s}^{A_m} A\left(\frac{A}{A_s}\right)^{-\alpha}\mathrm{d}A\right] & A^* \in [0, A_s] \\ \dfrac{C}{D}\displaystyle\int_{A^*}^{A_m} A\left(\frac{A}{A_s}\right)^{-\alpha}\mathrm{d}A & A^* \in [A_s, A_m] \\ 0 & A^* \in [A_m, \infty] \end{cases}$$
$$= \begin{cases} 1 - \dfrac{(1-\frac{\alpha}{2})A_s^{-\alpha}(A^*)^2}{A_m^{2-\alpha} - \frac{\alpha}{2}A_s^{2-\alpha}} & A^* \in [0, A_s] \\ 1 - \dfrac{(A^*)^{2-\alpha} - \frac{\alpha}{2}A_s^{2-\alpha}}{A_m^{2-\alpha} - \frac{\alpha}{2}A_s^{2-\alpha}} & A^* \in [A_s, A_m] \\ 0 & A^* \in [A_m, +\infty) \end{cases} \tag{A.5}$$

## Appendix B. Sensitivity of contact statistics to surface parameters

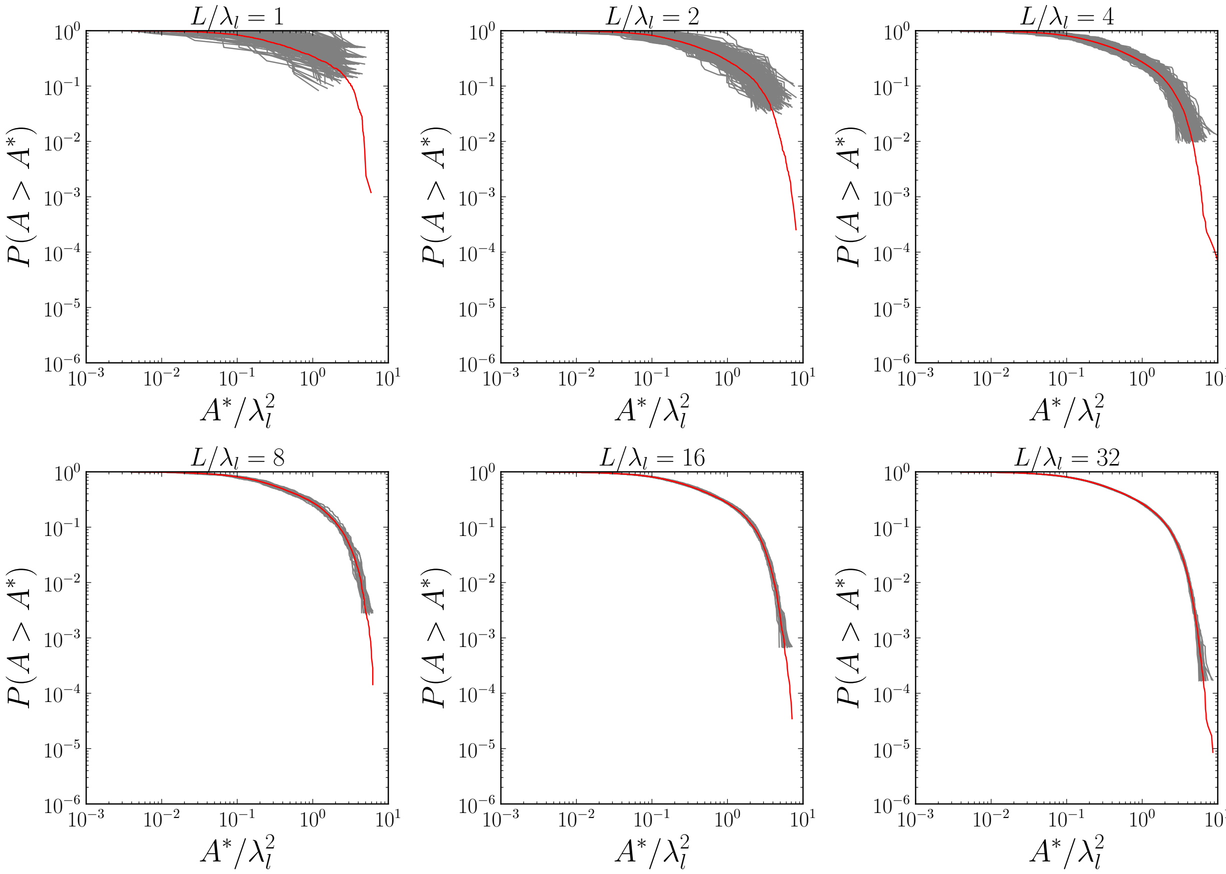


Figure B.1: **Influence of $L/\lambda_l$ on the complementary cumulative distribution function of contact-cluster areas.** Grey curves are results for each realization (20 in total), and red curves are ensemble averages. Surface sampled has $\lambda_l/\lambda_s = 8$ and $\lambda_s/\Delta l = 16$, so that only $L$ is varied. As $L/\lambda_l$ increases, the dispersion of the individual realizations decreases, and the behavior of the ensemble average approximates accurately the behavior of each realization. We also note that as $L/\lambda_l$ increases, the distributions converge to a limit distribution. For the simulations carried out in the rest of this paper, a value of $L/\lambda_l = 8$, which is a good compromise between required number of realizations and computational cost, was selected. Note: we analyze the cumulative distribution instead of probability density to remove any bias due to binning.

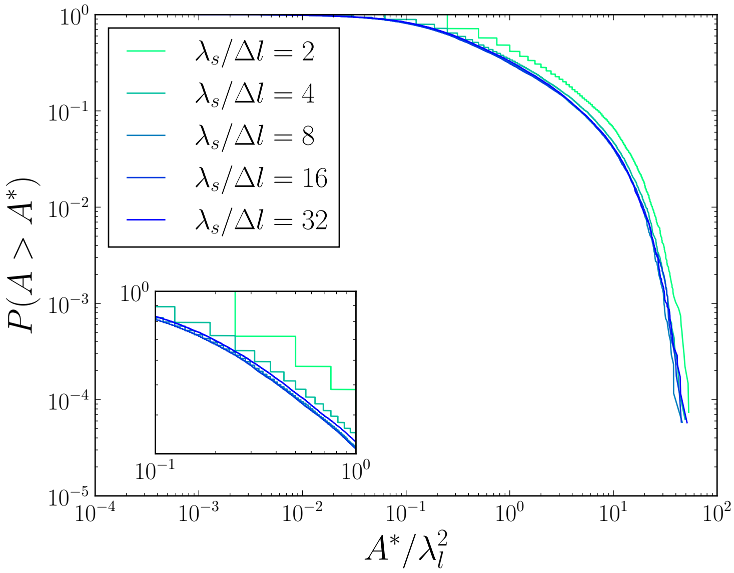


Figure B.2: **Influence of $\lambda_s/\Delta l$ on the complementary cumulative distribution function of contact-cluster areas.** Curves are ensemble averages of 20 realizations of a surface with $L/\lambda_l = 16$ and $\lambda_l/\lambda_s = 8$, so only $\Delta l$ is varied. As $\lambda_s/\Delta l$ is increased, the distributions converge to a limit distribution. Increasing $\lambda_s/\Delta l$ smoothens the distributions and reduces the systematic bias between the computed distribution and the limit of $\lambda_s/\Delta l \to \infty$. For simulations carried out in the main paper, a value of $\lambda_s/\Delta l = 8$ was selected, offering a reasonably low discretization bias, and making the simulations possible with our current code.

[1] Aghababaei, R., Warner, D. H., Molinari, J.-F., Jun. 2016. Critical length scale controls adhesive wear mechanisms. Nature Communications 7, 11816.
[2] Aghababaei, R., Warner, D. H., Molinari, J.-F., Jul. 2017. On the debris-level origins of adhesive wear. Proceedings of the National Academy of Sciences 114 (30), 7935–7940.
[3] Archard, J. F., Aug. 1953. Contact and Rubbing of Flat Surfaces. Journal of Applied Physics 24 (8), 981–988.
[4] Archard, J. F., Hirst, W., Aug. 1956. The Wear of Metals under Unlubricated Conditions. Proceedings of the Royal Society of London A: Mathematical, Physical and Engineering Sciences 236 (1206), 397–410.
[5] Burwell, J. T., Oct. 1957. Survey of possible wear mechanisms. Wear 1 (2), 119–141.
[6] Burwell, J. T., Strang, C. D., Jan. 1952. On the Empirical Law of Adhesive Wear. Journal of Applied Physics 23 (1), 18–28.
[7] Campañá, C., Aug. 2008. Using Green's function molecular dynamics to rationalize the success of asperity models when describing the contact between self-affine surfaces. Physical Review E 78 (2), 026110.
[8] Campañá, C., Müser, M. H., Robbins, M. O., 2008. Elastic contact between self-affine surfaces: Comparison of numerical stress and contact correlation functions with analytic predictions. Journal of Physics: Condensed Matter 20 (35), 354013.
[9] Challen, J. M., Oxley, P. L. B., Hockenhull, B. S., Sep. 1986. Prediction of Archard's wear coefficient for metallic sliding friction assuming a low cycle fatigue wear mechanism. Wear 111 (3), 275–288.
[10] Clauset, A., Shalizi, C. R., Newman, M. E. J., Nov. 2009. Power-Law Distributions in Empirical Data. SIAM Review 51 (4), 661–703.
[11] Colaço, R., Oct. 2009. An AFM study of single-contact abrasive wear: The Rabinowicz wear equation revisited. Wear 267 (11), 1772–1776.
[12] Das, S., Varalakshmi, K., Jayaram, V., Biswas, S. K., May 2007. Ultra Mild Wear in Lubricated Tribology of an Aluminium Alloy. Journal of Tribology 129 (4), 942–951.
[13] Davidesko, G., Sagy, A., Hatzor, Y. H., Mar. 2014. Evolution of slip surface roughness through shear. Geophysical Research Letters 41 (5), 2013GL058913.
[14] Dieterich, J. H., Kilgore, B. D., May 1996. Imaging surface contacts: Power law contact distributions and contact stresses in quartz, calcite, glass and acrylic plastic. Tectonophysics 256 (1–4), 219–239.
[15] Fleming, J. R., Suh, N. P., Aug. 1977. The relationship between crack propagation rates and wear rates. Wear 44 (1), 57–64.
[16] Greenwood, J. A., Williamson, J. B. P., Dec. 1966. Contact of Nominally Flat Surfaces. Proceedings of the Royal Society of London A: Mathematical, Physical and Engineering Sciences 295 (1442), 300–319.
[17] Griffith, A. A., Jan. 1921. VI. The phenomena of rupture and flow in solids. Phil. Trans. R. Soc. Lond. A 221 (582-593), 163–198.
[18] Hatchett, C., 1803. Experiments and Observations on the Various Alloys, on the Specific Gravity, and on the Comparative

Wear of Gold. Being the Substance of a Report Made to the Right Honourable the Lords of the Committee of Privy Council, Appointed to Take into Consideration the State of the Coins of This Kingdom, and the Present Establishment and Constitution of His Majesty's Mint. Philosophical Transactions of the Royal Society of London 93, 43–194.

[19] Hokkirigawa, K., Dec. 1991. Wear mode map of ceramics. Wear 151 (2), 219–228.

[20] Holm, R., 2000. Electric Contacts: Theory and Applications, 4th Edition. Springer, Berlin ; New York.

[21] Hsu, S. M., Shen, M., May 2004. Wear prediction of ceramics. Wear 256 (9–10), 867–878.

[22] Hu, Y., Tonder, K., Feb. 1992. Simulation of 3-D random rough surface by 2-D digital filter and fourier analysis. International Journal of Machine Tools and Manufacture 32 (1-2), 83–90.

[23] Hyun, S., Pei, L., Molinari, J.-F., Robbins, M. O., Aug. 2004. Finite-element analysis of contact between elastic self-affine surfaces. Physical Review E 70 (2), 026117.

[24] Hyun, S., Robbins, M. O., Oct. 2007. Elastic contact between rough surfaces: Effect of roughness at large and small wavelengths. Tribology International 40 (10–12), 1413–1422.

[25] Kato, K., Jul. 2000. Wear in relation to friction — a review. Wear 241 (2), 151–157.

[26] Kato, K., Adachi, K., 2001. Wear Mechanisms. In: Modern Tribology Handbook, bharat bhushan Edition. CRC Press, pp. 273–299.

[27] Liang, X., Lin, B., Han, X., Chen, S., Jun. 2012. Fractal analysis of engineering ceramics ground surface. Applied Surface Science 258 (17), 6406–6415.

[28] Majumdar, A., Bhushan, B., Apr. 1990. Role of Fractal Geometry in Roughness Characterization and Contact Mechanics of Surfaces. Journal of Tribology 112 (2), 205–216.

[29] Majumdar, A., Bhushan, B., Jan. 1991. Fractal Model of Elastic-Plastic Contact Between Rough Surfaces. Journal of Tribology 113 (1), 1–11.

[30] Mandelbrot, B. B., Jan. 1975. Stochastic models for the Earth's relief, the shape and the fractal dimension of the coastlines, and the number-area rule for islands. Proceedings of the National Academy of Sciences 72 (10), 3825–3828.

[31] Mandelbrot, B. B., Passoja, D. E., Paullay, A. J., Apr. 1984. Fractal character of fracture surfaces of metals. Nature 308 (5961), 721–722.

[32] Mischler, S., Muñoz, A. I., Jan. 2013. Wear of CoCrMo alloys used in metal-on-metal hip joints: A tribocorrosion appraisal. Wear 297 (1), 1081–1094.

[33] Müser, M. H., Dapp, W. B., Bugnicourt, R., Sainsot, P., Lesaffre, N., Lubrecht, T. A., Persson, B. N. J., Harris, K., Bennett, A., Schulze, K., Rohde, S., Ifju, P., Sawyer, W. G., Angelini, T., Esfahani, H. A., Kadkhodaei, M., Akbarzadeh, S., Wu, J.-J., Vorlaufer, G., Vernes, A., Solhjoo, S., Vakis, A. I., Jackson, R. L., Xu, Y., Streator, J., Rostami, A., Dini, D., Medina, S., Carbone, G., Bottiglione, F., Afferrante, L., Monti, J., Pastewka, L., Robbins, M. O., Greenwood, J. A., Dec. 2017. Meeting the Contact-Mechanics Challenge. Tribology Letters 65 (4), 118.

[34] Nayak, P. R., Jul. 1971. Random Process Model of Rough Surfaces. Journal of Lubrication Technology 93 (3), 398–407.

[35] Pei, L., Hyun, S., Molinari, J.-F., Robbins, M. O., Nov. 2005. Finite element modeling of elasto-plastic contact between rough surfaces. Journal of the Mechanics and Physics of Solids 53 (11), 2385–2409.

[36] Persson, B. N. J., Jun. 2006. Contact mechanics for randomly rough surfaces. Surface Science Reports 61 (4), 201–227.

[37] Persson, B. N. J., Albohr, O., Tartaglino, U., Volokitin, A. I., Tosatti, E., 2005. On the nature of surface roughness with application to contact mechanics, sealing, rubber friction and adhesion. Journal of Physics: Condensed Matter 17 (1), R1.

[38] Polonsky, I. A., Keer, L. M., Jul. 1999. A numerical method for solving rough contact problems based on the multi-level multi-summation and conjugate gradient techniques. Wear 231 (2), 206–219.

[39] Popov, V. L., Gervé, A., Kehrwald, B., Smolin, I. Y., Dec. 2000. Simulation of wear in combustion engines. Computational Materials Science 19 (1), 285–291.

[40] Power, W. L., Tullis, T. E., Weeks, J. D., Dec. 1988. Roughness and wear during brittle faulting. Journal of Geophysical Research: Solid Earth 93 (B12), 15268–15278.

[41] Rabinowicz, E., Aug. 1958. The effect of size on the looseness of wear fragments. Wear 2 (1), 4–8.

[42] Rabinowicz, E., 1995. Friction and Wear of Materials, 2nd Edition. Wiley, New York.

[43] Rabinowicz, E., Tabor, D., Sep. 1951. Metallic Transfer between Sliding Metals: An Autoradiographic Study. Proceedings of the Royal Society of London A: Mathematical, Physical and Engineering Sciences 208 (1095), 455–475.

[44] Riahi, A. R., Alpas, A. T., Aug. 2003. Wear map for grey cast iron. Wear 255 (1–6), 401–409.

[45] Scherge, M., Martin, J. M., Pöhlmann, K., Feb. 2006. Characterization of wear debris of systems operated under low wear-rate conditions. Wear 260 (4), 458–461.

[46] Stanley, H. M., Kato, T., Jul. 1997. An FFT-Based Method for Rough Surface Contact. Journal of Tribology 119 (3), 481–485.

[47] Svetlizky, I., Fineberg, J., May 2014. Classical shear cracks drive the onset of dry frictional motion. Nature 509 (7499), 205–208.

[48] Wang, Y., Hsu, S. M., Jul. 1996. Wear and wear transition modeling of ceramics. Wear 195 (1), 35–46.

[49] Yastrebov, V. A., Anciaux, G., Molinari, J.-F., Sep. 2012. Contact between representative rough surfaces. Physical Review E 86 (3).

[50] Yastrebov, V. A., Anciaux, G., Molinari, J.-F., 2017. On the accurate computation of the true contact-area in mechanical contact of random rough surfaces. Tribology International.

[51] Zhang, J., Alpas, A. T., Feb. 1997. Transition between mild and severe wear in aluminium alloys. Acta Materialia 45 (2), 513–528.

---